AIMS Materials Science

AIMS Materials Science, 4(1): 147-157.
DOI: 10.3934/matersci.2017.1.147
Received: 07 November 2016
Accepted: 10 January 2017
Published: 13 January 2017

http://www.aimspress.com/journal/Materials

Research article

Identification of slow relaxing spin components by pulse EPR techniques in graphene-related materials

Antonio Barbon* and Francesco Tampieri

Department of Chemical Science, University of Padova, Via Marzolo 1, 35131 Padova, Italy

* **Correspondence:** Email: antonio.barbon@unipd.it.

Abstract: Electron Paramagnetic Resonance (EPR) is a powerful technique that is suitable to study graphene-related materials. The challenging ability requested to the spectroscopy is its capability to resolve the variety of structures, relatively similar, that are obtained in materials produced through different methods, but that also coexist inside a single sample. In general, because of the intrinsic inhomogeneity of the samples, the EPR spectra are therefore a superposition of spectra coming from different structures. We show that by pulse EPR techniques (echo-detected EPR, ESEEM and Mims ENDOR) we can identify and characterize species with slow spin relaxing properties. These species are generally called *molecular states*, and are likely small pieces of graphenic structures of limited dimensions, thus conveniently described by a molecular approach. We have studied commercial reduced graphene oxide and chemically exfoliated graphite, which are characterized by different EPR spectra. Hyperfine spectroscopies enabled us to characterize the molecular components of the different materials, especially in terms of the interaction of the unpaired electrons with protons (number of protons and hyperfine coupling constants). We also obtained useful precious information about extent of delocalization of the molecular states.

Keywords: graphenic-related materials; RGO; exfoliated graphite; pulse EPR

1. Introduction

Graphene is nowadays one of the materials that is driving recent technological developments, with applications in different areas, like energetics [1], electronics [2], medicine and bioimaging [3,4], catalysis [5] and many more. A recent perspective review can be found in [6].

Besides the first method of production of graphene, based on the simple scotch-tape technique [7], a bunch of methodologies have been developed; chemical vapour deposition (CVD), reduction of graphene oxide (GO) obtained by the Hummers method [8] and exfoliation of graphite [9] are the most popular. Materials produced with these methods have a variety of properties which derive from the structural modifications, the eventual stacking of layers, the dimensionality [10] and the presence of defects [11].

This variety of structures, on one side, has generated the necessity to introduce a classification of the materials [6] and on the other side it has introduced the cogent need of a thorough characterization.

Most common techniques used for characterization of these materials are Raman spectroscopy [12], XRD [13] and microscopies (AFM, SEM, TEM) [14] which are used in particular to study properties like structure, number of stacked graphene layers, crystallinity, presence of defects, dimension of crystallites.

Electron paramagnetic resonance (EPR) was first applied for the study of graphene in 2009 by L. Ćirić et al. [15]. They found a continuous wave EPR (cw-EPR) spectrum composed by a single line with g-factor equal to 2.004, with slight variations on changing of the temperature. This line has been attributed to conduction electrons, as it has a reversed Curie temperature dependence, thus with a temperature (T) dependence of the magnetic susceptibility (χ) (related to the EPR intensity) with the form $\chi = const \cdot T$. The theory that explains this behavior was developed in the 50's by J.W. McClure [16], using graphene as a simplification of the structure of graphite. The lineshape of the cw-EPR spectra of conduction electrons in graphene flakes is Lorentzian (differently from bulk graphite where the skin effect due to the dimensionality of the system causes the line to be asymmetric [17]), with linewidths above 5 G in a wide temperature range, which corresponds to a transverse relaxation time T_2 of the order of 10^1 ns.

Because of the large variety of materials produced and studied, it became soon evident the contribution of edge states in determining some properties of graphene-like materials, in particular their magnetic properties [18] and, naturally, their influence on the spectrum of graphene. Edge states are associated to the limited extension of the crystallites, being better observed in nanostructured materials [19,20]. These are non-bonding states localized at the Fermi level [21] and are responsible for the paramagnetic contribution to the magnetization [22]. The behaviour of the electrons residing in these states is complicated by the presence of interactions between them and conduction electrons [23], as already observed in related materials like nanographites [20]. Different materials give different behaviours, either ferromagnetic or antiferromagnetic [24,25], and it appears that more research is needed in order to clarify the physics of the interactions. Nevertheless, the measurements indicate a general increase of the contribution of these states at low temperature with respect to conduction electrons; the lower limit is obviously determined by the exchange interaction value.

Beside the presence of conduction electrons and electrons in edge states, it is possible to observe electrons in so-called *molecular states*. These states were introduced some years ago [19] to indicate a variety of situations where electrons are located in islands at the edges of the flakes with a reduced extension of the spin distribution. Lineshapes are not Lorentzian [9] because of unresolved interactions with paramagnetic nuclei. This fact enables the use of electron spin echo techniques [26], which conveniently distinguish contributions characterized by the presence of inhomogeneously broadened spectra from those homogeneously broadened. With these techniques, it is also possible to apply a relaxation time filter for the detection of different species [27].

In general, electron spin echo intensities are affected by the delay between the pulses normally by functions of type $I(2\tau) = I_0 e^{-2\tau/T_M}$; here 2τ is the time distance between the first pulse and the echo, and T_M is the phase memory time, that, under certain conditions (ideal pulses, small tilt angle, very diluted sample [26–29]), gets close to T_2. For τ comparable to T_2 the echo is strongly quenched, and then only components with longer T_2 are visible. Indeed we used pulse EPR techniques to separate and characterize slow spin relaxing species, that are attributed to molecular states, characterized by slow spin relaxation. In this study we have considered two types of samples: reduced graphene oxide (RGO), as a standard material extensively studied, and graphene obtained by exfoliation of graphite with different chemical procedures. The main aim of the paper is to show the possibility to disentangling the EPR spectra of graphene-like material by exploiting the different relaxation properties of the different components.

2. Materials and Methods

We studied three different materials: two chemically exfoliated graphites (EK and EHK) and a commercial reduced graphene oxide as reference material (RGO). RGO was received from ACS Materials (MA, USA), labelled "Single layer Graphene" and used solid without further purification. Natural Madagascar graphite (SM), was kindly provided by Superior Graphite (Chicago, USA). Potassium metal, absolute ethanol, sulfuric acid and nitric acid were acquired from Sigma-Aldrich. All materials were used as received. Sample EK was obtained by intercalating potassium metal to Madagascar graphite, in order to obtain potassium graphite (KC_8). Subsequently ethanol was added. It reacted with potassium forming hydrogen gas that expanded the carbon layers. Sample EHK, was first intercalated by a mixture of sulfuric and nitric acids and thermally treated, before the intercalation with potassium and reaction with ethanol as sample EK. The details of the synthesis are described in reference [9].

The EPR measurements, cw and pulse, were obtained with an X-band Bruker ELEXSYS spectrometer, equipped with a dielectric resonator and a nitrogen/helium gas-flow cryostat for low temperature measurement. The samples were placed inside 2 or 3 mm ID quartz EPR tubes sealed under vacuum after full evacuation of adsorbed gases (normally overnight pumping). The EPR signals were followed as function of temperature from room temperature (290 K) down to almost the liquid helium temperature (10 K ca.). The field was calibrated using LiTCNQ for g-factor. Pulse experiments were performed using the standard pulse sequences. Hahn echo decay measurements (HD) were obtained by measuring the primary electron spin echo (ESE) intensity from a two-pulse experiment $\pi/2 - \tau - \pi - \tau - echo$ as function of the pulse delay, using a $\pi/2$ pulse of 16 ns. Two pulse electron spin echo envelope modulation (2p-ESEEM) spectra were obtained by Fourier transforming of the pure modulation component present in the HD, after a reconstruction (linear prediction singular value decomposition) of the signal not acquired during the dead time of the instrument, that was extended to 200 ns to avoid distortion in the echo decay profile. Echo-detected EPR (ED-EPR) spectra were obtained by recording the echo intensity of a fixed-delay ESE sequence as function of the magnetic field; we verified that the shape of the spectrum was independent from the value of the delay. The FT-EPR spectra were obtained after Fourier transformation of a free induction decay (FID) signal recorded using a simple $\pi/2$ pulse of 48 ns. The pulse ENDOR spectra were collected using an ENDOR dielectric resonator and an ENI A300RF power amplifier. The experiments were performed using the Mims sequence, $\pi/2 - \tau - \pi/2 - T - \pi/2 - \tau - echo$ with

a RF π pulse applied during the delay T [30,31]. We used a mw $\pi/2$ pulse of 20 ns, a RF π pulse of 10000 ns, $\tau = 1000$ ns and $T = 13000$ ns.

3. Results and Discussion

Graphene-like materials are intrinsically characterized by a large heterogeneity, thus their EPR spectra are typically a superposition of the spectra of different components present in the materials. The evolution of the cw-EPR spectra with the temperature of the samples has been previously reported in Ref. [9] where the analysis was conducted by considering the presence of two major components. We have observed that a change of the temperature induces a variation of the absolute and relative weight of the components; the linewidth also varies with the temperature.

On the base of the homogeneous linewidth values it is possible to estimate the relative T_2 values on the base of the well-known relation $T_2 = |\gamma_e \Gamma|^{-1}$, where γ_e is the free-electron magnetogyric ratio and its value is -1.761×10^{11} $s^{-1} \cdot T^{-1}$ and Γ is half the linewidth at half-height [32]. By using this relation, for the cw signals we deduct that, overall, spin-spin relaxation times are in the range of 1–20 ns as reported in Table 1.

Table 1. Spin-spin relaxation time T_2 for the two main components as obtained from the homogeneous linewidths of the simulated cw-EPR spectra at room temperature and at 80 K.

Sample	T = 290 K		T = 80 K	
	$T_{2,1}$ (ns)	$T_{2,2}$ (ns)	$T_{2,1}$ (ns)	$T_{2,2}$ (ns)
EK	1.7	5	11	5
EHK	11	5	13	4
RGO	13	4	20	4

We note that ESE-based experiments in solid state allows the determination of the phase memory time T_M values which are normally shorter than T_2. As a consequence, in pulse experiments the presence of an instrumental dead-time of about 200 ns prevents completely the observation of all the major components observed by cw-EPR.

We tried to record EDEPR, but only below 120 K ca. the formation of an echo could be observed for all samples. The species observed by pulse techniques are necessarily minor paramagnetic contributions, characterized by a long relaxation time, that are overlooked in the cw-EPR spectra.

We recall that at these low temperatures, on the basis of the analysis conducted in [9], the contribution to the cw-EPR coming from mobile electrons is strongly reduced in favour of electrons in edge states, for which the temperature dependence of these signals is a classical Curie law (rise of the intensity on going down with temperature).

We could not determine quantitatively the fraction of these minor components, but on the basis of the absolute echo intensity we can make a rough estimate that these components are below 10%.

Figure 1 reports the Hahn decay traces as function of pulse delay ($Time = 2\tau$) for the three samples showing a biexponential decay with a fast (300–400 ns) and a slow (1–3 μs) component [9].

In the figure the dead-time of the instrument is shown, within which the magnetization of the major components of the cw-EPR spectra are completely relaxed.

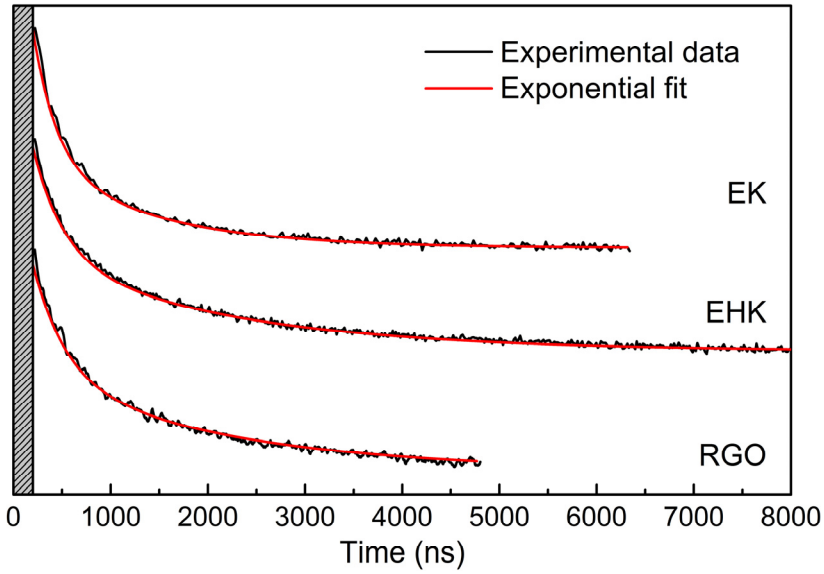

Figure 1. Normalized Hahn echo decay traces obtained for samples EK, EHK and RGO recorded at 80 K (black lines) as function of pulse delay ($Time = 2\tau$). The traces have been fitted using biexponential function (red lines). The grey rectangle indicates the dead-time of the instrument, where the magnetization of the major components of the cw-EPR spectrum decay before detection.

In order to obtain the spectral features of the slow relaxing components, giving rise to an echo, either EDEPR or FT-EPR techniques were used. Figures 2 and 3 report two examples of EDEPR spectra obtained for samples EK (Figure 2; the spectrum is representative of that of EHK, see [9]) and RGO (Figure 3). At first sight, EDEPR spectrum of EK exhibits a profile similar to that of the cw-EPR. Nevertheless an accurate analysis shows the differences in term of g-tensor and on the lineshape: the simulation of the EDEPR required the use of Gaussian lineshapes for all samples (see the simulations in Figure 2), as indication of the presence of unresolved hyperfine interactions between the electron and the paramagnetic nuclei; for samples EK and EHK line broadening was also due to g-anisotropy. The simulation parameters are reported in Table 2. At the lowest temperatures (below around 20 K), for RGO, having a narrow spectrum, it was also possible to acquire the FT-EPR spectrum. In analogy with the ESE-based experiments, a filter for separation of fast relaxing species is applied by starting the acquisition of the free induction decay (FID) after the instrument dead-time, a time sufficient to obtain a complete relaxation of the fast relaxing species. The delay was slightly extended in order to avoid distortion of the echo decay.

For RGO the difference between the EDEPR and the cw-EPR spectra is more evident, as the EDEPR spectrum of RGO is a single Gaussian with a relative narrow linewidth, whereas the spectra of the exfoliated graphites are the sum of two Gaussian components.

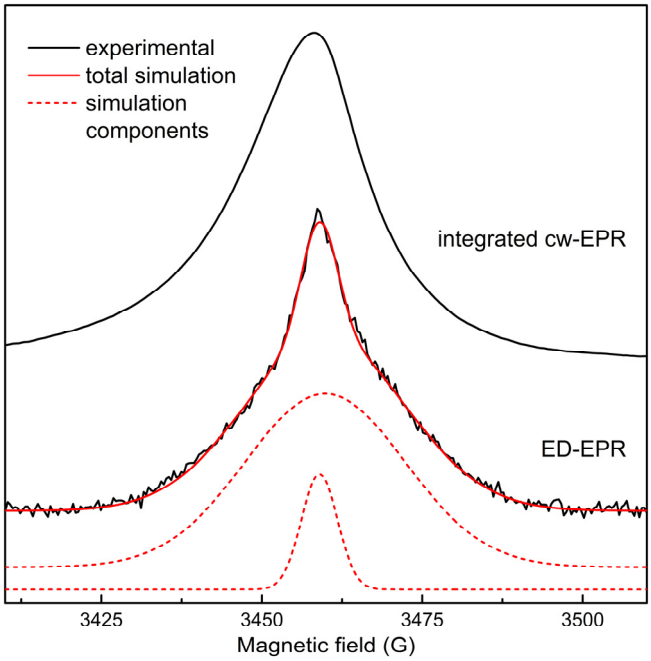

Figure 2. Integrated cw-EPR spectrum and EDEPR spectrum of sample EK at 80 K. For EDEPR $\tau = 200$ ns. The simulation of the EDEPR spectrum as sum of two Gaussian components is shown (continuous red line) together with the two separated components (dashed red lines). The parameters of the simulation are reported in Table 2.

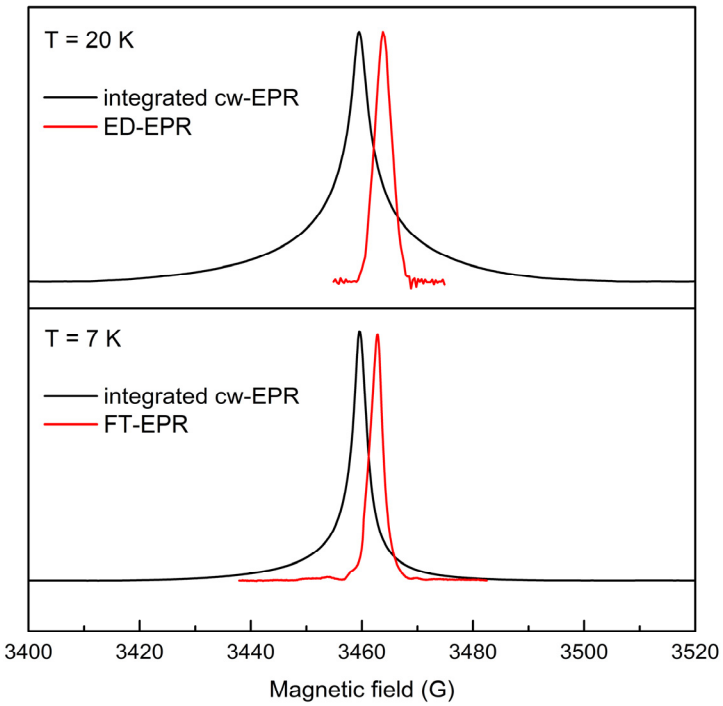

Figure 3. Top: ED-EPR spectra of sample RGO, recorded at 20 K. Bottom: FT-EPR of the RGO sample recorded at 7 K (red lines). In both spectra the black lines are the relative cw-EPR spectra in the integrated form.

Table 2. Relevant simulation parameters of the EDEPR spectra at 80 K. For each contribution *i*, the linewidth, the perpendicular (subscript label *a*) and parallel (subscript label *b*) components of the *g*-tensors are reported (isotropic or parallel g_{1a} and perpendicular g_{1b}). The relative abundance of the species (C_i) is indicated. A Gaussian lineshape was considered for all components.

Sample	$\%C_1$	g_{1a}	g_{1b}	Γ_1 (G)	g_{2a}	g_{2b}	Γ_2 (G)
EK*	13	2.0059	2.0034	2.5	2.0020	2.0097	11.8
EHK*	9.2	2.0058	2.0018	2.4	2.0040	2.0049	13.3
RGO*	100	2.0038	---	1.6	---	---	---

* simulation parameters taken from [9].

We further characterized the interactions between the unpaired electrons and the paramagnetic nuclei by using ESEEM and pulse ENDOR. These techniques enable to determine both the strength of the interaction and the type of interacting nuclei, as the observed bands, for relative small interactions, are centered around the free Larmor frequency of the different nuclei. We expected the presence of paramagnetic nuclei (^{1}H and ^{13}C) ^{1}H, having at the magnetic field of the experiments (0.34 T) a Larmor frequency of 14.5 MHz ca., and ^{13}C with a Larmor frequency of 3.6 MHz ca.. For protons the hyperfine coupling constant (hcc) is of particular value as in such π-type systems is directly connected to the spin density at the bound carbon atom on the basis of the well-known McConnell theory [32], and then to the extension of the π-density.

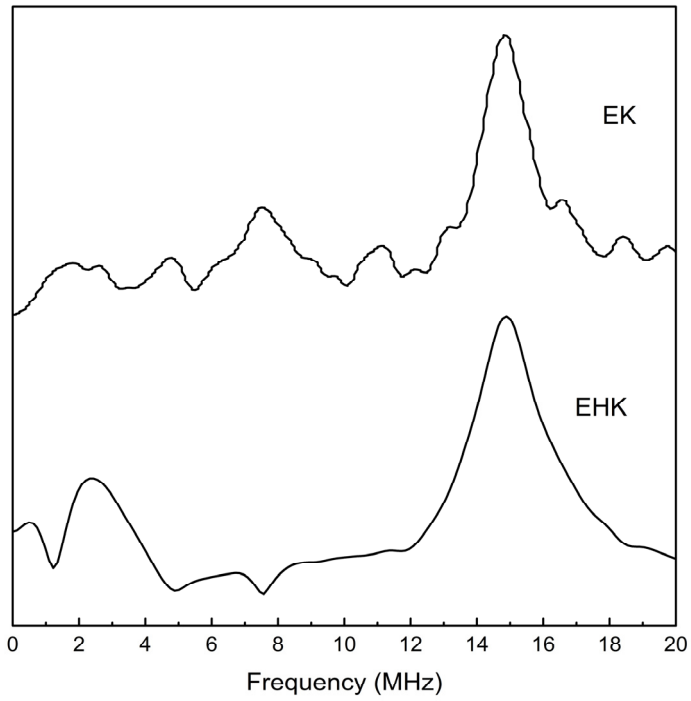

Figure 4. 2p-ESEEM spectra of samples EH and EHK recorded at 80 K and at a magnetic field of 3460 G. At this field the nuclear frequencies of protons and ^{13}C are respectively 14.7 MHz and 3.7 MHz.

In Figure 4, we show the 2p-ESEEM spectra for EK and EHK. Because for RGO the modulation in the HD decay was very mild, to improve it we collected the 3p-ESEEM, that slightly improved; the spectrum is displayed in the Supporting Information, Figure S2. The spectra of samples EK and EHK are relatively similar and are characterized by a very evident band centered at the proton resonance frequency. Another band relative to the ^{13}C nuclei is better observed for the EHK sample. The signal for sample EK is comparable with the noise for sample EK, but is evident at 5 K (see Figure S1 in Supplementary Information). The proton signal, for the two samples, has a full width at half maximum of 2.4 MHz for sample EK and 3.0 MHz for sample EHK meaning that the hcc with the protons is about 1.4 G and 1.8 G respectively. RGO sample showed weak bands of both ^{13}C and protons. It is to be stressed that nuclei with low Larmor frequency give intrinsically deeper modulation depths [28].

For samples EK and RGO we then collected the Mims ENDOR spectra (Figure 5), a suitable technique to detect small hyperfine interactions up to 5 MHz, and where, in general, distortion effects are less present. Unselected microwave pulses produced signals from both components observed by EDEPR. In the two cases it was possible to note a proton band.

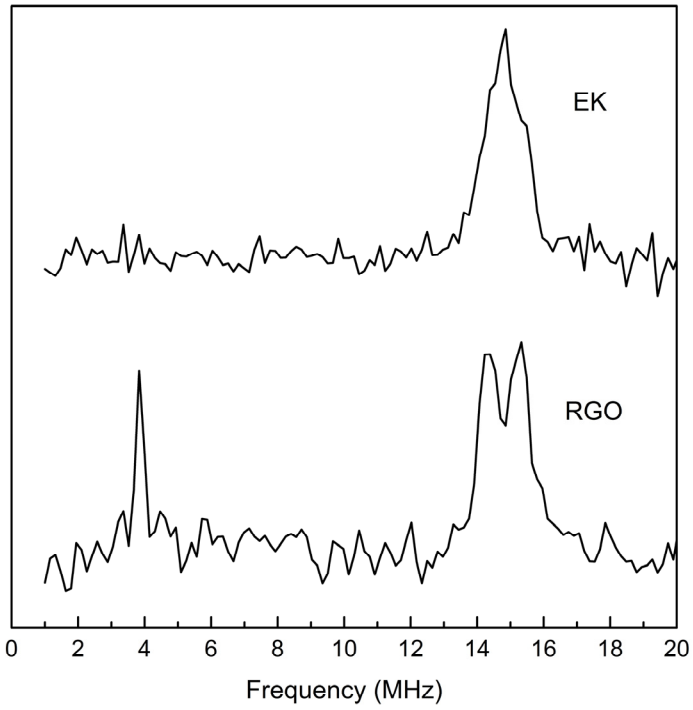

Figure 5. Mims ENDOR spectra of samples EK and RGO recorded at 20 K at a field of 3470 G. At this field the nuclear frequencies of protons and ^{13}C are respectively 14.8 MHz and 3.7 MHz.

The most obvious information obtained from the ESEEM and ENDOR spectra is that the components detected by pulse techniques are composed of both protons and carbon atoms, and consequently we can deduce that they are small graphene-like flakes terminated by protons. The relative content of protons and ^{13}C atoms in EK and EHK is rather similar with slightly larger ^{13}C band for EHK, whereas the protons in RGO are substantially less than the other samples. We can

estimate the average dimension of these fragments by comparing hcc relative to protons, that is about 1.4 and 1.8 G for EK and EHK, respectively, with the values in reference π-systems, like coronene and circumcoronene, having a different π extension of 24 and 54 atoms respectively. From literature, for coronene we found an isotropic coupling constant of about 1.5 G and for circumcoronene of about 0.6 G [33,34].

By comparing these data with those obtained from exfoliated graphites and RGO we conclude:

1. For RGO, this molecular states are composed of fragments of graphene about 25 carbon atoms large, with a lateral dimension of about 1 nm.
2. In RGO, the content of protons interacting with the unpaired electron is lower, but this is not surprising by taking into account the structure or RGO, which is in general composed of graphene islands connected by hydrocarbon chains, and that can be decorated by different groups (alcohol, acids, aldehydes), which lower the content of protons directly bound to the π-system.
3. The high content of protons in the EK and EHK samples is likely due to the saturation of the particle edges entirely with protons, as generated by reaction in a very reductive environment during the reaction with potassium. The presence of g-anisotropy suggests the presence of stacks of layers, or the smaller dimension of these particles with respect to RGO.

4. Conclusion

By studying graphene-like materials by pulse EPR techniques it is possible to obtain paramagnetic components that are overlooked in the cw-EPR spectra, as they are of small intensity.

Characterization of these components by ESEEM and ENDOR enabled us to get information on the structure of these components. In particular, it was possible to investigate the chemical composition of the surroundings of the unpaired electrons by looking at the signals of coupled nuclei and to deduce the average size of the flakes by analyzing the proton signal in the ESEEM spectra. We note that, because of the absence on nuclear magnetic moment, oxygen could not be detected. Different results were obtained for EK and EHK samples with respect to RGO. The lower content of protons in RGO is due to the decoration of the graphene fragments in this type of material, with several organic functional groups beside protons.

Conflict of Interest

The authors declare that there is no conflict of interest regarding the publication of this paper.

References

1. Quesnel E, Roux F, Emieux F, et al. (2015) Graphene-based technologies for energy applications, challenges and perspectives. *2D Mater* 2: 030204.
2. Chen A, Hutchby J, Zhirnov V, et al. (2014) *Emerging nanoelectronic devices*, John Wiley & Sons.
3. Mattei TA, Rehman AA (2014) Technological developments and future perspectives on graphene-based metamaterials: a primer for neurosurgeons. *Neurosurgery* 74: 499–516.
4. Ray S (2015) *Applications of graphene and graphene-oxide based nanomaterials*, William Andrew.

5. Higgins D, Zamani P, Yu A, et al. (2016) The application of graphene and its composites in oxygen reduction electrocatalysis: a perspective and review of recent progress. *Energ Environ Sci* 9: 357–390.
6. Ferrari AC, Bonaccorso F, Fal'Ko V, et al. (2015) Science and technology roadmap for graphene, related two-dimensional crystals, and hybrid systems. *Nanoscale* 7: 4598–4810.
7. Novoselov KS, Geim AK, Morozov SV, et al. (2004) Electric field effect in atomically thin carbon films. *Science* 306: 666–669.
8. Hummers Jr WS, Offeman RE (1958) Preparation of graphitic oxide. *J Am Chem Soc* 80: 1339–1339.
9. Tampieri F, Silvestrini S, Riccò R, et al. (2014) A comparative electron paramagnetic resonance study of expanded graphites and graphene. *J Mater Chem C* 2: 8105–8112.
10. Ching W, Rulis P (2012) *Electronic Structure Methods for Complex Materials: The orthogonalized linear combination of atomic orbitals*, Oxford University Press.
11. Yoon K, Rahnamoun A, Swett JL, et al. (2016) Atomistic-Scale Simulations of Defect Formation in Graphene under Noble Gas Ion Irradiation. *ACS Nano* 10: 8376–8384.
12. Ferrari A, Meyer J, Scardaci V, et al. (2006) Raman spectrum of graphene and graphene layers. *Phys Rev Lett* 97: 187401.
13. Badenhorst H (2014) Microstructure of natural graphite flakes revealed by oxidation: limitations of XRD and Raman techniques for crystallinity estimates. *Carbon* 66: 674–690.
14. Pardini L, Löffler S, Biddau G, et al. (2016) Mapping atomic orbitals with the transmission electron microscope: Images of defective graphene predicted from first-principles theory. *Phys Rev Lett* 117: 036801.
15. Ćirić L, Sienkiewicz A, Nafradi B, et al. (2009) Towards electron spin resonance of mechanically exfoliated graphene. *Phys Status Solidi B* 246: 2558–2561.
16. McClure J (1957) Band structure of graphite and de Haas-van Alphen effect. *Phys Rev* 108: 612.
17. Wagoner G (1960) Spin resonance of charge carriers in graphite. *Phys Rev* 118: 647.
18. Nair R, Sepioni M, Tsai I, et al. (2012) Spin-half paramagnetism in graphene induced by point defects. *Nat Phys* 8: 199–202.
19. Tommasini M, Castiglioni C, Zerbi G, et al. (2011) A joint Raman and EPR spectroscopic study on ball-milled nanographites. *Chem Phys Lett* 516: 220–224.
20. Barbon A, Brustolon M (2012) An EPR Study on Nanographites. *Appl Magn Reson* 42: 197–210.
21. Makarova T, Palacio F (2006) *Carbon based magnetism: an overview of the magnetism of metal free carbon-based compounds and materials*, Elsevier Science.
22. Osipov VY, Shames A, Enoki T, et al. (2009) Magnetic and EPR studies of edge-localized spin paramagnetism in multi-shell nanographites derived from nanodiamonds. *Diam Relat Mater* 18: 220–223.
23. Augustyniak-Jabłokow MA, Tadyszak K, Maćkowiak M, et al. (2012) ESR study of spin relaxation in graphene. *Chem Phys Lett* 557: 118–122.
24. Tadyszak K, Augustyniak-Jabłokow MA, Więckowski AB, et al. (2015) Origin of electron paramagnetic resonance signal in anthracite. *Carbon* 94: 53–59.
25. Makarova T, Shelankov A, Zyrianova A, et al. (2015) Edge state magnetism in zigzag-interfaced graphene via spin susceptibility measurements. *Sci Rep* 5: 13382.

26. Collauto A, Mannini M, Sorace L, et al. (2012) A slow relaxing species for molecular spin devices: EPR characterization of static and dynamic magnetic properties of a nitronyl nitroxide radical. *J Mater Chem* 22: 22272–22281.
27. Marrale M, Longo A, Brai M, et al. (2011) Pulsed EPR analysis of tooth enamel samples exposed to UV and γ-radiations. *Radiat Measur* 46: 789–792.
28. Brustolon M, Barbon A (2003) Pulsed EPR of Paramagnetic Centers in Solid Phases, In: Lund A *EPR of Free Radicals in Solids*, Springer, 39–93.
29. Barbon A, Brustolon M, Maniero A, et al. (1999) Dynamics and spin relaxation of tempone in a host crystal. An ENDOR, high field EPR and electron spin echo study. *Phys Chem Chem Phys* 1: 4015–4023.
30. Mims W (1965) Pulsed ENDOR experiments. *Proc R Soc Lond A* 283: 452–457.
31. Schweiger A, Jeschke G (2001) *Principles of pulse electron paramagnetic resonance*, Oxford University Press.
32. Weil JA, Bolton JR (2007) *Electron paramagnetic resonance: elementary theory and practical applications*, John Wiley & Sons.
33. Lewis IC, Singer L (1965) Electron spin resonance of radical cations produced by the oxidation of aromatic hydrocarbons with $SbCl_5$. *J Chem Phys* 43: 2712–2727.
34. Janata J, Gendell J, Ling C, et al. (1967) Concerning the anion and cation radicals of corannulene. *J Am Chem Soc* 89: 3056–3058.

AIMS Press